nature communications

Article

https://doi.org/10.1038/s41467-024-55404-6

Counterintuitive DNA destabilization by monovalent salt at high concentrations due to overcharging

Received: 26 May 2024

Accepted: 11 December 2024

Published online: 02 January 2025

Check for updates

Chen Zhang[1,6], Fu-Jia Tian[1,6], Hong-Wei Zuo[2,6], Qi-Yuan Qiu[2], Jia-Hao Zhang[1], Wei Wei[1], Zhi-Jie Tan[3], Yan Zhang[4] ✉, Wen-Qiang Wu[5] ✉, Liang Dai[2] ✉ & Xing-Hua Zhang[1] ✉

Monovalent salts are generally believed to stabilize DNA duplex by weakening inter-strand electrostatic repulsion. Unexpectedly, our force-induced hairpin unzipping experiments and thermal melting experiments show that LiCl, NaCl, KCl, RbCl, and CsCl at concentrations beyond ~1 M destabilize DNA, RNA, and RNA-DNA duplexes. The two types of experiments yield different changes in free energy during melting, while the results that high concentration monovalent salts destabilize duplexes are common. The effects of these monovalent ions are similar but also have noticeable differences. From 1 M to 4 M, DNA duplex is destabilized by about 0.3 k_BT/bp and the melting temperature decreases by about 10 °C. Our all-atom simulations reveal this effect is caused by overcharging, where excessive ion absorption inverts the effective DNA charge from negative to positive. Furthermore, our coarse-grained simulations obtain a phase diagram that indicates whether DNA overcharging occurs at a given cation valence and concentration. These findings challenge the traditional belief that DNA overcharging occurs only with multivalent ions and have significant implications for polyelectrolyte theory, DNA nanomaterials, DNA nanotechnology, and DNA biophysics.

Ion-nucleic acid interactions play essential roles in biological processes, because nucleic acids, including DNA and RNA, carry high-density negative charges (see a review in ref. 1). One important role of ions, such as Na^+ and K^+, is screening the repulsions among negative charges in nucleic acids[2–6]. Without such screening, DNA duplex would be unstable, and RNA folding would not occur due to the strong repulsions in nucleic acids[1].

In this work, our experiments surprisingly find that monovalent cations destabilize DNA duplexes when salt concentration (c_{salt}), is beyond a critical concentration (c^*_{salt}). Such destabilization by ions is opposite to the stabilization caused by electrostatic screening[7–9]. And such DNA destabilization occurs for LiCl, NaCl, KCl, RbCl, and CsCl. Furthermore, the destabilization by monovalent ions also occurs for other nucleic acids (NA) including RNA and RNA-DNA hybrid (RDH) duplexes, which suggests the phenomenon is general, independent of the structural details of NA duplexes.

Previous studies have observed many salt effects on DNA that go beyond electrostatic screening. For example, multivalent ions can induce DNA-DNA attraction[10,11], which is manifested by DNA condensation, and reversal of DNA electrophoretic direction[12]. However, these experimental phenomena occur only with multivalent ions, such as cobalt hexamine ($CoHex^{3+}$), but not with monovalent ions. Theories

[1]Hubei Key Laboratory of Cell Homeostasis, College of Life Sciences, Renmin Hospital of Wuhan University, Wuhan University, Wuhan, China. [2]Department of Physics, City University of Hong Kong, Hong Kong, China. [3]Department of Physics, Wuhan University, Wuhan, China. [4]Department of Clinical Laboratory, Renmin Hospital of Wuhan University, Wuhan, China. [5]School of Life Sciences, State Key Laboratory of Crop Stress Adaptation and Improvement, Henan University, Kaifeng, China. [6]These authors contributed equally: Chen Zhang, Fu-Jia Tian, Hong-Wei Zuo. ✉e-mail: peneyyan@whu.edu.cn; wuwenqiang@henu.edu.cn; liangdai@cityu.edu.hk; zhxh@whu.edu.cn

have been developed to explain multivalent ion-induced DNA-DNA attraction and DNA charge inversion observed in experiments[13,14]. According to the theory based on the Wigner crystal, the interactions between multivalent ions are so strong that they form a strongly correlated liquid or Wigner crystal, which causes DNA-DNA attraction and DNA charge inversion[13,14]. According to this theory, the interactions between monovalent ions are not strong enough to induce a Wigner crystal. Simulations have observed DNA charge inversion[15], and DNA-DNA attraction induced by multivalent ions[16]. In terms of monovalent effects beyond electrostatic screening, simulations have observed DNA-DNA attraction induced by high concentrations of NaCl[17]. This phenomenon is different from the DNA destabilization with monovalent ions, because the former is about inter-DNA interaction, while the latter is about intra-DNA interaction[18]. In addition, DNA overcharging induced by monovalent ions has been observed in coarse-grained (CG) simulations and theoretical calculations[19]. In these simulations and calculations, DNA was modeled as a cylinder and water molecules were not considered. It is not sure that the phenomenon in such a simple model can be applied to realistic DNA molecules. After two decades of this work, no experimental results have confirmed that DNA overcharging can occur with monovalent ions. Whether DNA overcharging by monovalent ions can occur remains unclear.

DNA thermal melting experiments by Tomac et al. [20] and Khimji et al. [2] observed that DNA duplex is destabilized at high concentrations of Na^+. Khimji et al. [2] did not discuss the mechanism of DNA destabilization because their focus was on the effect of polyanions on DNA stability. Their experiments used only one monovalent ion, Na^+. It is unclear whether any ion-specific effects cause DNA destabilization under high salt concentrations. Later, a theoretical work by Maity, Singh, and Singh[5] reproduced the DNA destabilization at high salt concentrations by assuming the effective base-pairing hydrogen bonds weaken at high salt concentrations. This assumption has not yet been validated.

In this work, we perform precise and systematic measurements for DNA, RNA, and RDH duplex stabilities across wide ranges of c_{salt} for LiCl, NaCl, KCl, RbCl, and CsCl. The experiments constantly show duplex destabilization by high concentrations of monovalent ions. Furthermore, we reveal that such duplex destabilization is caused by overcharging using extensive all-atom molecular dynamics (MD) and CG Langevin dynamics simulations, as well as Wigner crystal theory. In addition, we discovered that overcharging can also occur for ssDNA through experiments and simulations.

Results

Monovalent cations at high concentrations destabilize DNA duplexes in single-molecule experiments

We first measured the stabilities of NA duplexes by unzipping short NA hairpins using magnetic tweezers (MT) experiments (Fig. 1a, b), similar to previous works[21–24], while we focused on the variation of the NA duplexes stability with monovalent salt concentrations. For each salt condition, we first measured the extension of the NA construct through a force-cycle containing a stretching process followed by a relaxing process. The NA hairpin unfolded during stretching and refolded during relaxing, which provided the unfolding and refolding forces (arrows, Fig. 1d), respectively. Within the range from the refolding force to the unfolding force, we searched for a transition force, f^*, where the folded and stretched states of the NA hairpin had the same probability (Fig. 1e). The free energy cost of hairpin unfolding equals the change in the external potential, $f^*\Delta L$ (Fig. 1f), where ΔL is the change in the DNA extension during the hairpin unfolding (Supplementary Fig. 1a). The transition is between the duplex state and the stretched state, and we denote the free energy cost as ΔG_{SD}. Note that varying salt concentration affects the refractive index of the buffer (up to 4%). We have considered this factor in the measurement of ΔL using a previous method[25]. Ultimately, we found that ΔL very weakly depends on the salt condition (Supplementary Fig. 1b).

Figure 1g shows f^* reaches a peak at a critical salt concentration, which is denoted as c^*_{salt}. The values of c^*_{salt} are always between 1 M and 2 M. Figure 2a shows NA duplex stabilities as functions of c_{salt}, which is calculated as $\Delta G_{SD} = f^*\Delta L$. Because we focus on the dependence of ΔG_{SD} on c_{salt}, we shift the curves to offset the peak values of ΔG_{SD} in Fig. 2b for NaCl (a similar plot for KCl is shown in Supplementary Fig. 2). From c^*_{salt} to 4 M, DNA duplex is destabilized by about $0.3\,k_BT$/bp. Such magnitude of duplex destabilization roughly equals the case from c^*_{salt} to 0.3M. Similar results were observed for RNA for five salt types (Fig. 2c, d). The values of c^*_{salt} for RNA are typically slightly lower than those for DNA. Under a given high c_{salt}, the magnitude of destabilization for RNA is smaller than the case of DNA. The differences between RNA and DNA are possibly caused by different charge densities and ion distribution patterns[26] (Supplementary Fig. 3). Previous ion counting experiments have also observed that ion distributions around RNA and DNA are different[1,27].

Measurement of duplex stability by thermal melting

We measured the melting temperature (T_m) of NA duplexes at various c_{salt} using a fluorescence quenching test, as detailed in the "Methods" section (Fig. 3 and Supplementary Fig. 4). In the duplex state, the BHQ1 quencher on one strand effectively suppressed the proximate FAM fluorescence on the complementary strand. We raised the temperature incrementally at a rate of 0.1 °C/s. As the NA duplex gradually melted and the FAM strand separated from the BHQ1 strand, we observed a corresponding increase in fluorescence intensity. The peak of the derivative of the fluorescence intensity determined the T_m under each salt condition[28].

As shown in Fig. 3b, T_m exhibits a non-monotonic change with c_{salt}, in agreement with the MT results in Fig. 1g. DNA destabilization at high c_{salt} consistently occurs for different DNA lengths from 12 to 400 bp and different GC percentages in thermal melting experiments (Supplementary Figs. 5 and 6). From these curves, we determined the critical salt concentrations, c^*_{salt}, corresponding to the maximum melting temperature. The values of c^*_{salt} are also between 1 and 2 M for all three NA duplexes and four types of monovalent salts, except for CsCl whose c^*_{salt} is below 1 M. The smaller c^*_{salt} for CsCl may be caused by stronger binding of Cs^+ to DNA than other cations.

The curves in MT experiments (Fig. 1g) are smoother and the error bars are smaller than those in thermal melting experiments (Fig. 3b). It is worth noting that the conformational transitions in MT and thermal melting experiments are slightly different (Fig. 3c). In MT experiments, NA hairpins transition between the folded duplex state and unfolded stretched state under tension, and the free energy difference is denoted as ΔG_{SD}. In thermal melting experiments, NA duplexes transit between the duplex state and a single-stranded random-coiled state, and the free energy difference is denoted as ΔG_{CD}. As shown in Fig. 3c, we have $\Delta G_{SD} = \Delta G_{CD} + \Delta G_{SC}$, where ΔG_{SC} is the free energy difference between the stretched state and coil state.

The value of ΔG_{SC} can be estimated through the integration of the force-extension curve $\Delta G^{chain}_{SC} = \int_{z_c}^{z_s} f\,dz$ from the coil state to the stretched state. Here, z_s and z_c are the extensions of the stretched and coil states, respectively, and f is the stretching force at a given extension, z. After approximating ssDNA as a worm-like chain[29], the dependence of the force on the extension is described by the Marko–Siggia equation $f = \frac{k_BT}{L_p}\left[\frac{1}{4(1-z/L)} - \frac{1}{4} + \frac{z}{L}\right]$. Here, L_p is the ssDNA persistence length, $L = Na$ is the ssDNA contour length, $N = 64$ is the number of nucleotides for DNA hairpin in MT experiments, and $a \approx 0.564$ nm is the contour length per nucleotide[30,31]. Previous experiments have obtained $L_p \approx 0.94$ nm, 1.08 nm, and 1.6 nm at 1 M, 0.5 M, and 0.1 M NaCl, respectively. Based on the Marko–Siggia equation and $f^* = 12.5$, 14.4, and 15 pN at 0.1, 0.5, and 1 M NaCl, we can obtain the values of z_c. Eventually, we obtained $\Delta G_{SC} = \Delta G^{chain}_{SC}/28 \approx 0.72$, 0.89, and

https://doi.org/10.1038/s41467-024-55404-6

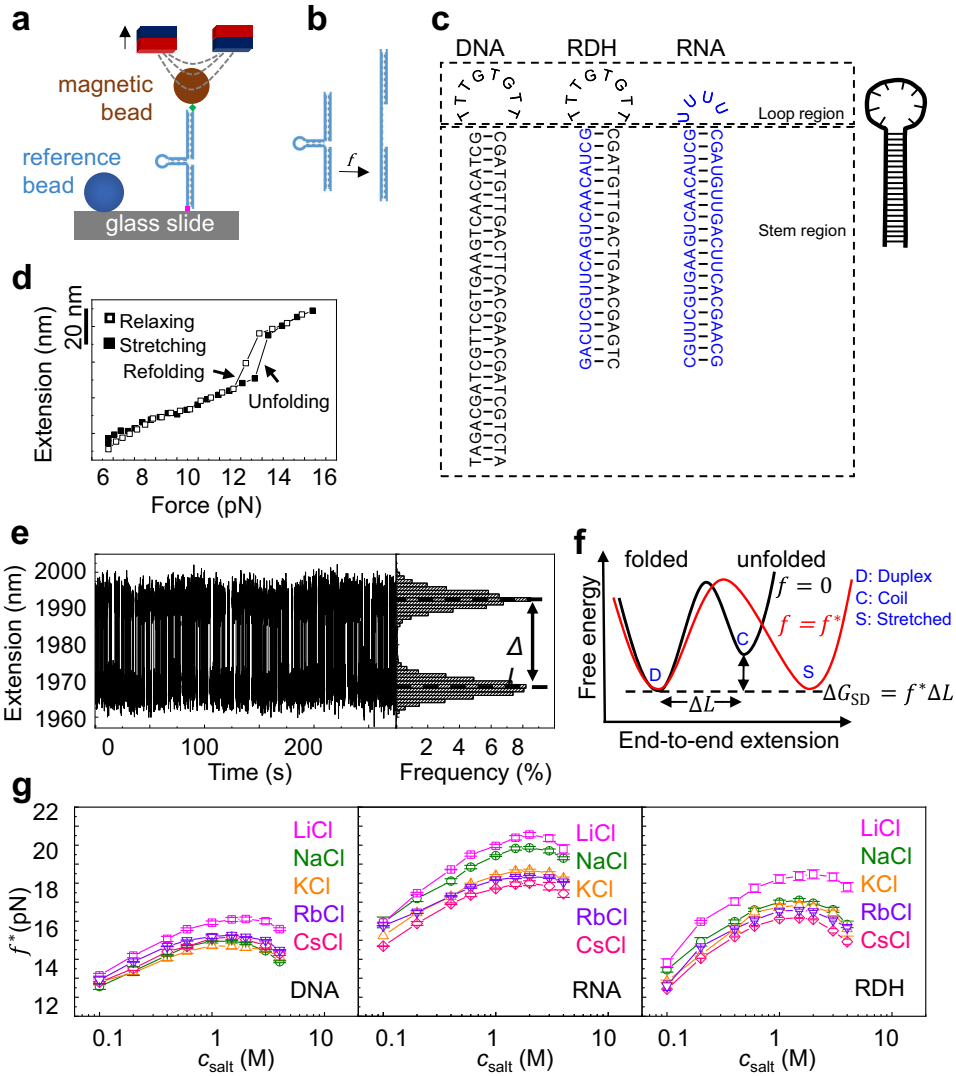

Fig. 1 | Measurement of NA duplex stability by MT experiments. Source are provided as a Source Data file. **a** Manipulation of NA hairpin using magnetic tweezers. **b** The NA hairpin is unfolded by the external force. **c** Illustration of the construct of three types of NA hairpins. Black for DNA bases and blue for RNA bases. **d** The unfolding and folding of an NA hairpin are indicated by abrupt changes in DNA extension during stretching and relaxing, respectively. **e** At the transition force f^*, the NA hairpin hops between the folded and stretched states with equal probability. **f** The free energy difference between the folded and unfolded hairpin. **g** Transition force as a function of salt concentration. The averages and standard errors from several molecules (four for CsCl and three for other ions) are plotted as data points and error bars.

0.95 k_BT/bp at 0.1, 0.5, and 1 M NaCl, correspondingly. Here, 28 is the number of base pairs of the DNA stem region in MT experiments. As illustrated in Fig. 3c, we expect $\Delta G_{SD} \approx \Delta G_{SC} + \Delta G_{CD}$. To examine this relationship, we calculated ΔG_{CD} using the nearest-neighbor model[32] and obtained $\Delta G_{CD} \approx 2.77\,k_BT$/bp at 1 M NaCl (Supplementary Method 1). With $\Delta G_{SD} \approx 3.53\,k_BT$/bp at 1 M NaCl from Fig. 2a and $\Delta G_{SD} \approx 0.95\,k_BT$/bp from the Marko–Siggia equation, we find that at 1 M NaCl, $\Delta G_{SC} + \Delta G_{CD} = 0.95 + 2.77 = 3.72\,k_BT$/bp, which is close to $\Delta G_{SD} \approx 3.53\,k_BT$/bp and confirms $\Delta G_{SD} \approx \Delta G_{SC} + \Delta G_{CD}$.

The increase of ΔG_{SC} with c_{salt} likely explains why the peak locations in Fig. 3b, i.e. c^*_{salt}, are generally smaller than the peak locations in Fig. 1g, considering that MT and thermal melting experiments correspond to ΔG_{SD}, and ΔG_{CD}, respectively, which differ by ΔG_{SC}.

The value of ΔG_{SC} depends not only on c_{salt}, but may also depend on the ion species. Ions may mediate intra-strand interaction in the random-coiled state and thus affect the effective ssDNA persistence length or make the force-extension curve deviate from the worm-like chain behavior[29]. For example, the smaller ΔG_{CD} for Na^+ and Cs^+ at high concentrations in Fig. 3b may be caused by greater intra-strand attraction mediated by Na^+ and Cs^+, which enhances the dependence of ΔG_{SC} on c_{salt}.

Mechanism of DNA duplex destabilization by monovalent ions

We propose that DNA duplex destabilization at high concentrations of monovalent salts is caused by DNA overcharging. In the following paragraphs, we will elaborate on this mechanism and provide evidence of this mechanism.

As c_{salt} increases, more and more counterions are absorbed on DNA and the effective DNA charge, q_{eff}, undergoes the transition from $q_{eff} < 0$ to $q_{eff} = 0$ and eventually to $q_{eff} > 0$. Here, $q_{eff} = 0$ means that the absorbed counterions carry the same amount but opposite charges as DNA, and DNA is effectively neutral. Under the condition of $q_{eff} = 0$, inter-strand electrostatic repulsion vanishes, and duplex stability is maximized. The condition of $q_{eff} > 0$ is referred to as DNA overcharging which reintroduces inter-strand electrostatic repulsion and reduces duplex stability. It is worth noting that q_{eff} corresponds to the total charges of DNA and ions within a certain short distance

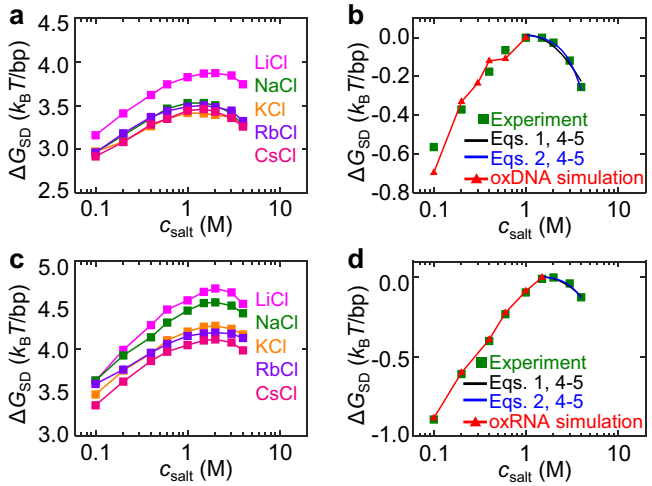

Fig. 2 | Comparison of experimental and simulation results. In MT experiments, the averages and standard errors from three molecules are plotted as data points and error bars. In MD simulations, the averages and standard errors from five equal intervals after equilibrium are plotted as data points and error bars. Source data are provided as a Source Data file. **a** The free energy difference between duplex and stretched single-stranded DNA states (ΔG_{SD}) as a function of salt concentration (c_{salt})) from MT experiments. **b** Variation of ΔG_{SD}, $\Delta\Delta G_{SD}$. The red curve is obtained from oxDNA simulation. **c**, **d** Similar results for RNA duplex stability and the red curve are obtained from oxRNA simulation. In (**b**) and (**d**), all experimental curves are shifted to make $\Delta\Delta G_{SD} = 0$ at c^*_{salt} for the salt type of NaCl, and the black curves are calculated from Eqs. 1, 4–5, and the blue curves from Eqs. 2, 4–5.

around DNA, because the total charges of DNA and all ions, i.e., the entire system, are always zero.

Simulations of DNA with monovalent ions

While DNA overcharging with high-valent ions has been observed in experiments[12] and explained by theory[13,14], DNA overcharging by monovalent ions is much less explored[19] and whether it can occur remains unclear. To quantitatively understand it, we performed three types of simulations with different resolutions, (i) all-atom MD simulations, (ii) oxDNA simulations, and (iii) CG Langevin dynamics simulations, as each simulation method has its own advantages and disadvantages. All-atom MD simulations can capture DNA overcharging but cannot capture the equilibrium transition of DNA strand separation. The oxDNA simulation is based on a CG DNA model whose resolution is lower than all-atom but higher than typical CG simulations[33]. The oxDNA simulations can capture the equilibrium transition of DNA strand separation but cannot capture DNA overcharging because there are no explicit ion particles in oxDNA simulations, and the effect of ion particles is considered through Debye screening. Our CG Langevin dynamics simulations, which are described in the "Methods" section, can dramatically improve computational efficiency and allow freedom to vary ion parameters but cannot capture many effects caused by water molecules, such as ion hydration. CG simulations are suitable for building a phase diagram of DNA overcharging.

We first present oxDNA simulation results. The red curve in Fig. 2b shows that oxDNA simulation can quantitatively capture the effect of c_{salt} on DNA duplex stability in the range of $c_{salt} < c^*_{salt}$ within the framework of the classic Debye screening, which supports that the variation of electrostatic interactions, rather than hydrogen bonds and base stacking, is the primary factor for the variation of DNA duplex stability within the c_{salt} range we consider here. Similar oxRNA simulations were performed and the results agree with experiments for $c_{salt} < c^*_{salt}$ (red curve in Fig. 2d). Note that the entire oxDNA (as well as oxRNA) parameterization is based on implicit ions with the Debye screening to reproduce a double-helical DNA structure with properties close to experimental results. Due to the absence of explicit ions, the oxDNA model cannot capture DNA overcharging by ions.

Next, we present all-atom MD simulations of a DNA duplex with NaCl, KCl, or CsCl. Our simulations reveal DNA overcharging in three aspects. First, we calculated q_{cyl}, the total charge of DNA atoms, Na^+, and Cl^- within a cylinder around DNA (Fig. 4a). For $c_{salt} \lesssim 1$ M, q_{cyl} is always negative, as expected from mean-field theory. However, for $c_{salt} \gtrsim 1$ M, q_{cyl} becomes positive at 1 nm $\lesssim r_{cyl} \lesssim$ 2 nm, which indicates DNA overcharging (Fig. 4b). For each c_{salt}, we recorded the maximum of q_{cyl}, which is denoted as q^{max}_{cyl}. The radial distances corresponding to q^{max}_{cyl} usually located at the first or second layer of ions absorbed on DNA. Figure 4c shows that when $c_{salt} > c^*_{salt}$, q^{max}_{cyl} increases roughly linearly with c_{salt}. Here, q^{max}_{cyl} is normalized for one base pair. According to the theory by Shklovskii et al. [13,14], the dependence of q^{max}_{cyl} on c_{salt} can be approximated by

$$q^{max}_{cyl} \approx k_q \ln(c_{salt}/c^*_{salt}) \tag{1}$$

Here, k_q is a fitting parameter. See more about Eq. 1 in Supplementary Method 2. As shown by the blue line in Fig. 4c, the fit of Eq. 1 to our simulation results yield $k_q = 0.163$ and $c^*_{salt} = 1.02$ M. Because the simulation data in Fig. 4c appears to follow a linear relationship, we also fit the data by

$$q^{max}_{cyl} \approx 0.074(c_{salt} - 1\,\mathrm{M}) \tag{2}$$

Note that the above linear equation is just for convenient usage, not based on rigorous mathematical simplification of Eq. 1.

Second, from the same simulation results of monovalent ion distribution, we calculated the electric field around DNA using Gauss's law, i.e., the strength of the electric field at r_{cyl} determined by q_{cyl}. Integration of the electric field over the radial distance, we obtained the electric potential around DNA, Φ_E (Fig. 4d). For $c_{salt} \lesssim 1$ M, Φ_E is always negative as expected from mean-field theory. For $c_{salt} \gtrsim 1$ M, Φ_E becomes positive at 1 nm $\lesssim r_{cyl} \lesssim$ 2 nm, which indicates DNA overcharging. For each c_{salt}, we recorded the maximum of Φ_E which is denoted as Φ^{max}_E. Figure 4e shows that Φ^{max}_E also increases with c_{salt} linearly after the critical concentration

$$\Phi^{max}_E \approx 1.509(c_{salt} - 1\,\mathrm{M}) \tag{3}$$

Alternatively, we can approximate Φ^{max}_E from q^{max}_{cyl} in Eq. 2. By approximating the thickness of the overcharging layer as 0.71 nm, we can obtain $\Phi^{max}_E \approx 2.13(c_{salt} - 1\,\mathrm{M})$ from Eq. 2, which is close to the result in Eq. 3. Note that due to Gauss's law, the linear behavior of the accumulated charge in Eq. 2 can lead to a linear behavior of the electrical potential.

Third, the radial distributions of Na^+ and Cl^- in Fig. 4f reveal DNA overcharging. The concentration of Na^+ at $r_{cyl} \approx 1.5$ nm is less than the Na^+ concentration far from DNA, indicating a positive electric potential at $r_{cyl} \approx 1.5$ nm. Similarly, the concentration of Cl^- at $r_{cyl} \approx 1.5$ nm is larger than the Cl^- concentration far from DNA.

To quantify the effect of overcharging on DNA strand-strand electrostatic interaction, we make several crude approximations. First, we use q^{max}_{cyl} to approximate the effective DNA charge per nucleotide. Second, we calculate the electrostatic interaction between two charges separated by a distance of 2 nm (the inter-strand P–P distance or DNA diameter)

$$E_0 \approx \frac{\left(q^{max}_{cyl} e\right)^2}{4\pi\varepsilon_0\varepsilon_{DNA} r} \approx \left(q^{max}_{cyl}\right)^2 \times 3.5\,k_B T \tag{4}$$

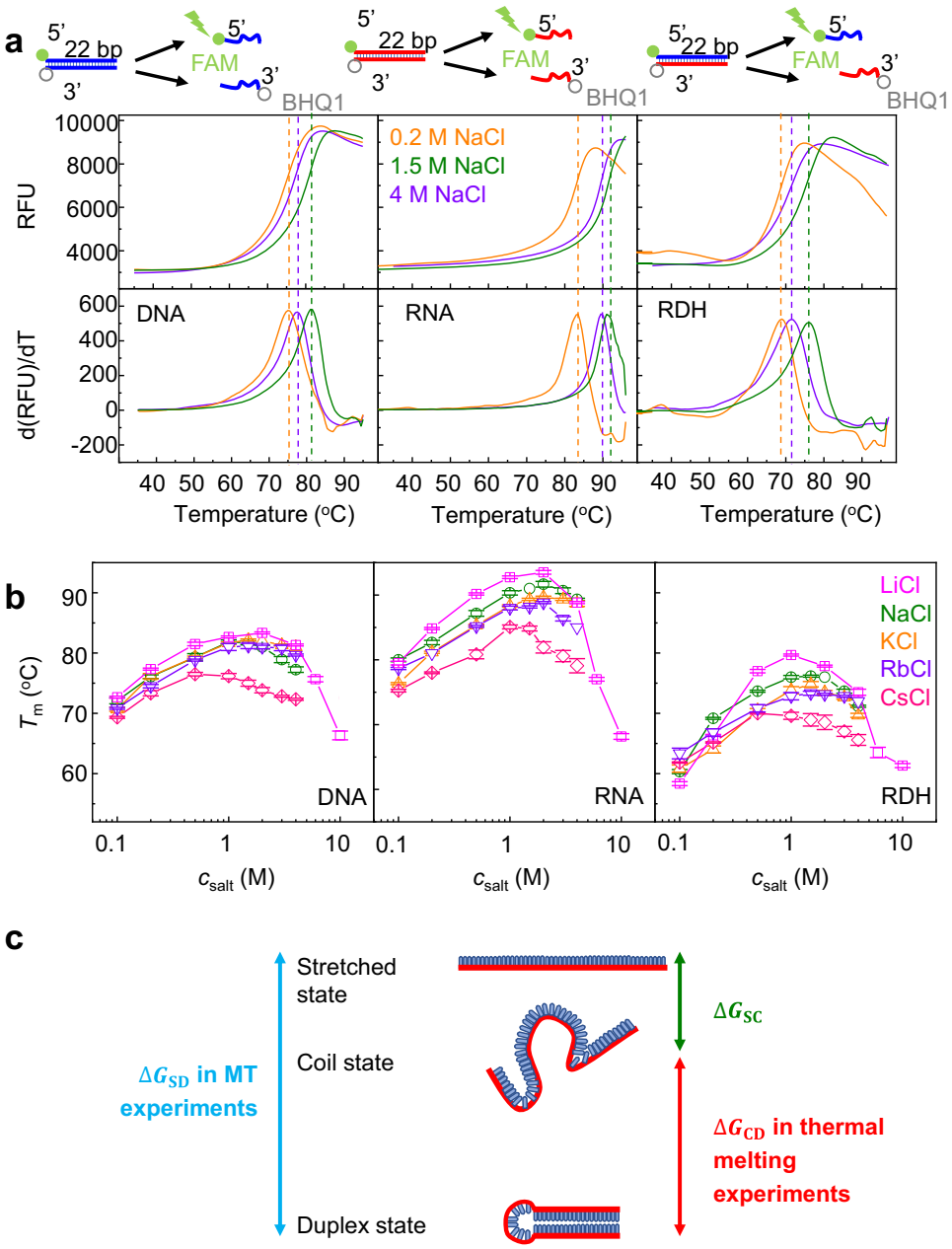

Fig. 3 | Measurement of NA duplex stability by thermal melting. Source data are provided as a Source Data file. **a** Representative melting curves obtained from a fluorescence quenching test. The top panels are the fluorescence intensity as a function of temperature, and the bottom panels are the derivative of fluorescent intensity versus temperature. **b** Melting temperature T_m as functions of c_{salt}. The averages and standard errors from several independent experiments (six for NaCl and three for other ions) are plotted as data points and error bars. **c** Two different transitions in MT and thermal melting experiments.

Here, e is the elementary charge, ε_0 is the vacuum permittivity, $\varepsilon_{DNA} = 8$ is the dielectric constant inside DNA[34], and $r = 2$ nm is the distance between two charges or the DNA diameter. We use the unit of k_BT for an easy comparison with experimental results in Fig. 2b.

The above calculation makes many approximations. Accordingly, we add a coefficient k_{fit}

$$E_{elec} \approx k_{fit} E_0 \tag{5}$$

Here, E_{elec} is the effect of DNA overcharging on inter-strand electrostatic interaction. The fit of Eq. 5 to the experimental results yields $k_{fit} = 1.4$, as shown by the black curve in Fig. 2b. One reason that causes $k_{fit} > 1$ is that the calculation of E_0 only considers the charge-charge interaction within a base pair, and actually the charge on a DNA strand can interact with all charges on the other DNA strand.

We did similar all-atom MD simulations for DNA in other monovalent salts. We obtained $q_{cyl}^{max} = 0.102\ln(c_{salt}/0.97\,\text{M})$ and $k_{fit} = 1.7$ with KCl (Supplementary Figs. 2 and 7) and $q_{cyl}^{max} = 0.122\ln(c_{salt}/0.96\,\text{M})$ and $k_{fit} = 1.6$ with CsCl (Supplementary Figs. 8 and 9). We also carried out similar all-atom MD simulations and analysis for RNA with NaCl (Supplementary Fig. 10) and obtained the black curve in Fig. 2d, which explains RNA duplex destabilization by monovalent ions. For RNA with NaCl, we obtained $q_{cyl}^{max} = 0.077\ln(c_{salt}/1.49\,\text{M})$ and $k_{fit} = 5.9$. These results suggest that NA duplexes overcharging with monovalent ions is a common phenomenon. Please see Supplementary Table 1 for the determined Eqs. 1–3 and 5 for different monovalent ions on DNA.

https://doi.org/10.1038/s41467-024-55404-6

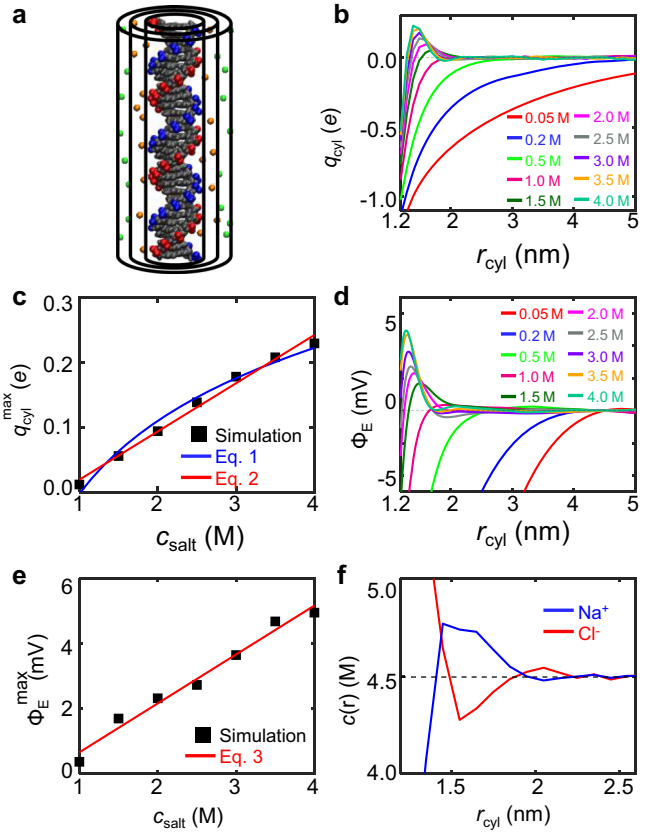

Fig. 4 | Ion distribution around the DNA from MD simulations. Source data are provided as a Source Data file. **a** Total charge, q_{cyl}, within a cylinder around DNA. The smallest cylinder has a radius of 1 nm, corresponding to DNA radius. The middle cylinder has a radius of 1.5 nm, corresponding to the position of the maximum overcharging. The largest cylinder has a radius of 2 nm, where the ion concentrations approach the bulk values. **b** q_{cyl} as a function of the cylindrical radius. **c** Maximum of q_{cyl}, q_{cyl}^{max}, as a function of NaCl concentration. **d** Electric potential, Φ_E, as a function of radial distance. **e** Maximum of Φ_E, Φ_E^{max}, as a function of NaCl concentration. **f** Radial distribution of Na^+ and Cl^- at 4.5 M NaCl.

Phase diagram of DNA overcharging with *n*-valent ions

The DNA overcharging with monovalent and high-valent ions inspires us to think about the criterion of DNA overcharging. What is the minimum ion valence that can induce DNA overcharging? To find the answer, we used CG simulations, which greatly accelerate simulations and allow for freedom to vary ion parameters (Fig. 5a). In these CG Langevin dynamics simulations, DNA is modeled as a charged rod with diameter, D_{rod} = 1.8 nm. The linear charge density of the rod is $-1e$ per 0.17 nm. Ions are modeled as hard spheres with different diameters, D_i = 0.3, 0.35, or 0.4 nm. We examined whether DNA overcharging occurs by analyzing the charge distribution and the electric potential around the DNA rod. When the monovalent ion concentration is greater than 1.6 M, DNA overcharging occurs (Supplementary Fig. 11 and Supplementary Method 3). Although the CG simulations ignore explicit water molecules and DNA structural details, we found that the CG simulations with suitable parameterization can quantitatively capture DNA overcharging observed in all-atom MD simulations (Fig. 5d).

From systematic CG simulation results, we obtained a phase diagram for the conditions of DNA overcharging (Fig. 5e). The critical concentrations of Mg^{2+} and Ca^{2+} where T_m reverses were obtained by thermal melting experiments (Supplementary Fig. 12). For a lower cation valence, c_{salt}^* is higher. Our theoretical phase boundary for D_i = 0.4 nm (red line in Fig. 5e) agrees with our experimental results for monovalent ions, Li^+, Na^+, K^+, Rb^+, and Cs^+. Our theoretical phase boundaries are above the experimental results for divalent ions, Mg^{2+} and Ca^{2+}, possibly because the hydrated ion diameters of Mg^{2+} and Ca^{2+} are larger than 0.4 nm. Our theoretical phase boundaries are close to a previous experimental result[12] for $CoHex^{3+}$. For a realistic salt solution, there is an upper limit of c_{salt}, which is the saturated salt concentration. When we set the maximum c_{salt} as 3 M, the minimum ion valence for DNA overcharging is about 0.8 for short DNA segments with straight rod conformations.

The reason for DNA overcharging has been investigated in previous studies[13,14,35,36]. It has been proposed that the excluded volume interaction between cations causes the positional correlations of cations around DNA. This correlation leads to an arrangement of cations where the cations of the second layer interlace with the cations of the first layer around DNA, resembling a crystal. Such arrangement significantly weakens the repulsions between cations in the first and second layers and allows excessive cations on the second or following layers, which results in DNA overcharging. In this mechanism, the excluded volume interaction between cations plays a crucial role in DNA overcharging, supported by the fact that the modified Poisson-Boltzmann equation considering the excluded volume interaction between cations can reproduce overcharging[36]. Our CG simulations also find that increasing ion diameter can reduce the minimum salt concentration for DNA overcharging, as seen by comparing the blue, black, and red curves in Fig. 5e. As shown in Fig. 5f, with the decrease of ion diameter, the overcharging electric potential decreases toward zero. Additionally, our CG simulations demonstrate the Φ_E^{max} of DNA overcharging appears to have a universal dependence on $c_{salt}D_i^2$ (Fig. 5g), which indicates the critical role of the excluded volume interaction of ions in DNA overcharging.

Discussion

Due to the high charge density of DNA, salt concentration strongly affects DNA stability. It is generally believed that monovalent ions weaken DNA-DNA electrostatic interactions by Debye screening and hence enhance DNA duplex stability. In contrast to the common belief, our experiments reveal that high concentrations of monovalent salts destabilize DNA duplexes. This counterintuitive behavior, consistent across DNA, RNA, and RDH duplexes and various monovalent salts (LiCl, NaCl, KCl, RbCl, and CsCl), points to a universal physical phenomenon rather than duplex-structure-specific or ion-specific effects. Our all-atom and CG simulations showed this destabilization is caused by DNA overcharging. The magnitude of DNA destabilization by overcharging is significant, which can be $0.3\,k_BT$ per base pair. Such magnitude decreases the melting temperature by about 10 °C.

The physical mechanism for DNA overcharging has been investigated previously using the Wigner crystal model[14]. In the classical mean-field treatment, when DNA charges are fully compensated by absorbed counterions, DNA cannot attract additional counterions because the absorbed counterions repel the additional counterions. The mean-field treatment assumes absorbed counterions distribute continuously on the DNA surface, while in real cases, counterions are discrete and may form a crystal-like structure on the DNA surface when the repulsions between counterions are strong. The crystal-like structure weakens the repulsions between absorbed counterions and other counterions, which allows neutralized DNA to absorb additional counterions. Please see Supplementary Method 2 and Supplementary Fig. 13 for the theoretical calculation of DNA overcharging using this theory and a simplified explanation for DNA overcharging, respectively. It is worth pointing out that Wigner crystal theory was developed for multivalent ions because the strong repulsions among multivalent ions favor the formations of crystal-like structures. Here, we applied the theory to monovalent ions and found the functional form, the logarithmic function in Eq. 1, seems to work, but the quantitative values, such as c_{salt}^*, deviate greatly from the prediction of the

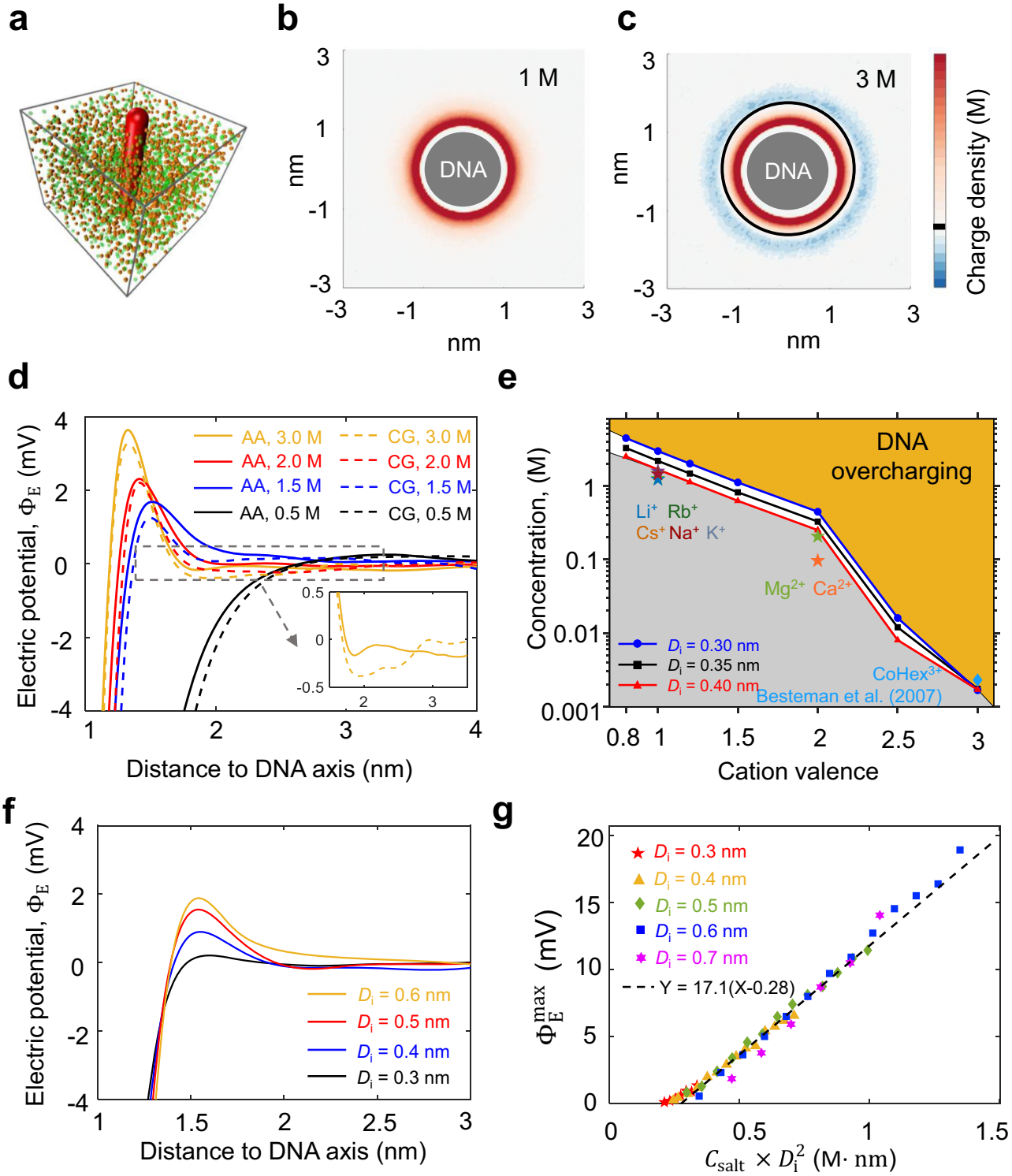

Fig. 5 | Criterion of DNA overcharging. Source data are provided as a Source Data file. **a** Coarse-grained simulation setup. **b** Diagram of charge distribution around DNA at 1 M NaCl from CG simulations. **c** Diagram of DNA overcharging from CG simulations with a DNA diameter of 2 nm and an ion diameter of 0.3 nm. **d** Electric potential, Φ_E, as a function of radial distance obtained from all-atom and CG MD simulations. **e** Phase diagram of DNA overcharging. The symbols represent experimental data from our work and a previous study[12]. Ions are modeled as hard spheres with different diameters, D_i. **f** The overcharging electric potential for different ion diameters. **g** Maximum of Φ_E, Φ_E^{max} versus $c_{salt} \times D_i^2$ for different ion diameters.

theory. Such deviation is not surprising, because monovalent ions do not form a Wigner crystal, as shown by the liquid-like structure in Fig. 4f. In addition to the Wigner crystal theory, a previous study has added two salt-dependent energetic terms for inter-strand interaction to capture DNA destabilization under high salt concentrations[5] (Supplementary Fig. 14 and Supplementary Method 4).

DNA overcharging is supported by several DNA phenomena observed in the literature. First, DNA overcharging is evidenced by the

reversal of the electrophoretic direction of DNA with high-valent ($n \geq 3$) ions[12]. Under normal salt conditions, DNA carries negative charges and migrates toward the anode. When $CoHex^{3+}$ exceeds a critical concentration ($c^*_{salt} \approx 1mM$), DNA absorbs excessive $CoHex^{3+}$ ions and migrates toward the cathode[12].

Second, DNA overcharging can weaken the attraction between two double-stranded DNA molecules. Previous experiments have observed that with the increasing concentration of high-valent ions such as $CoHex^{3+}$, DNA first condensed, indicating DNA-DNA attraction, and then dissolved at even higher concentrations, indicating DNA-DNA repulsion[10,11,37]. Previous theoretical studies have explained it by following mechanisms[13,14,35]. There are two contributions of electrostatic interactions between two DNA molecules. The first contribution is the classical electrostatic repulsion between two DNA molecules, which can be understood in the mean-field treatment or Debye screening. The second contribution is the like-charge attraction caused by ion correlation. With the increase of high-valent ion concentration, the first contribution switches from repulsion to zero and eventually to repulsion again due to DNA overcharging. After assuming the second contribution does not vary much with c_{salt}, DNA overcharging can explain the experimental phenomena of DNA dissolution, condensation, and re-dissolution with the increase of c_{salt}. Similarly, DNA condensation resists the maximum stretching force around the critical salt concentration of charge inversion because inter-DNA electrostatic repulsion vanishes[12,38]. A difference between those experiments and our experiment is that these experiments deal with the interaction between two double-stranded DNA fragments, while our work focuses on the inter-strand interaction within a duplex. Nevertheless, DNA overcharging should strengthen the repulsion within a duplex or between DNA duplexes. Our experiments and all-atom simulations also observed single-stranded DNA overcharging at large c_{salt} (Supplementary Figs. 15 and 16 and Supplementary Method 5).

DNA destabilization induced by monovalent ions has significant implications in polyelectrolyte theory, DNA nanomaterials, DNA nanotechnology, and DNA biophysics. First, DNA destabilization induced by monovalent ions inspires us to clarify the criterion of DNA overcharging. It is generally believed that DNA overcharging occurs for multivalent ions but not monovalent ions. Our experimental and simulation results refresh the understanding. Broadly speaking, the precise experimental results of DNA help advance polyelectrolyte theory. In the past decades, DNA, as a model polymer and a model polyelectrolyte, has greatly facilitated the advance of polymer physics theory in terms of providing quantitative results, such as the scaling behavior of single polymers in confinement[39–41], and polyelectrolyte theory, such as like-charge attraction and overcharging[11,14]. There are several advantages for DNA as a model polymer and a model polyelectrolyte, including mature biotechnology to prepare high-quality DNA samples[42,43] and well-established single-DNA experiments by MT[44].

Second, DNA has been widely applied in nanomaterial design, which takes advantage of the base-pairing attraction to achieve well-defined nanostructures[45–47]. Such nanomaterial design requires DNA duplex formation, and the material stability depends on DNA duplex stability. Our quantitative results of DNA duplex stability as a function of salt concentration can be applied to rationally control the stability of such nanomaterials.

Third, high concentrations of monovalent salts, such as LiCl and KCl, are commonly used in DNA-nanopore experiments in order to enhance the precision of electrical signals[48–50]. In addition, strand separation is often involved in nanopore experiments[51,52]. In such cases, DNA destabilization induced by monovalent salt at high concentrations should be considered.

Lastly, DNA destabilization under high salt concentration may be biologically relevant. For example, some halophilic archaea cells prefer a high salt environment and can even grow on NaCl crystals[53].

In conclusion, we summarize the overall results of this work, (i) precisely measuring DNA, RNA, and RDH destabilization by Li^+, Na^+, K^+, Rb^+, Cs^+; (ii) demonstrating DNA destabilization by high concentrations of monovalent ions is a common phenomenon, not ion-specific; (iii) revealing that such DNA destabilization is caused by DNA overcharging using extensive all-atom and CG simulations, as well as Wigner crystal theory. Our results have both fundamental and practical values, (i) Fundamentally, we advance the polyelectrolyte theory of overcharging using DNA as a model polyelectrolyte. We highlight that the single-DNA technique can achieve a high precision (~0.01 pN & 1 nm) that is unachievable in traditional experiments for other polyelectrolytes. (ii) Practically, our systematical experimental data of DNA, RNA, and RHD duplexes stabilization under various salt concentrations act as the table of physical-chemical data for nucleic acids, which can be used in many bio-nanotechnological applications, such as DNA origami, and DNA-nanopore sequencing.

Method

Buffer solutions

We prepared the near-saturation concentration of monovalent salt mother liquor which undergoes filtration, DEPC treatment, and autoclaving. The concentration of the mother liquor was 10 M for LiCl, 5 M for NaCl, 4 M for KCl, 5 M for RbCl, and 5 M for CsCl. Before each experiment, we used DEPC-treated deionized water to dilute the mother liquor to different salt concentrations. We used a buffer system comprising a final concentration of 10 mM Tris-HCl to ensure a consistent pH of 7.5.

MT experiments

Each NA (DNA, RNA, or RDH) hairpin construct was labeled with digoxigenin at one end and labeled with biotin at the other end (Fig. 1a). The loop regions have 8 nucleotides for DNA and RDH hairpins but 4 nucleotides for RNA hairpin. Because RNA transitions between folded and unfolded states more slowly than DNA under equilibrium, we designed shorter loop regions for RNA to accelerate the transition rate[21,24]. A previous study[21] has found that reducing the loop-region length has no obvious effect on ΔG_{SD} shown in Fig. 1f. See the illustrations of hairpins in Fig. 1c. We made the DNA and RNA constructs by one-sided PCR[54] and made the RDH construct by ligation (Supplementary Fig. 17 and Supplementary Method 6).

We sequentially coated the piranha-cleaned glass slides with 1% APTES, 2% glutaraldehyde, 1 mg/mL anti-digoxigenin and passivated the slides with 2% bovine serum albumin. After coating glutaraldehyde on the glass slides, we attached the polystyrene microbeads as references. In a flow cell, we attached the digoxigenin-labeled end of the NA hairpin construct to the anti-digoxigenin-coated glass slide and attached its biotin-labeled end to a streptavidin-coated paramagnetic microbead (Dynabeads M-270). We used a pair of neodymium magnets to exert force to stretch the NA hairpin construct and controlled the stretching force using a linear motor (L-509, Physik Instrument). We viewed the microbeads by a 100× oil immersion objective (Olympus), captured the images with a CCD camera (MER2-230-168U3M, Daheng Imaging), and calculated the positions of the microbeads based on their diffraction pattern[55]. We conducted the experiments in an ultra-clean room with a stable temperature of 22 °C.

Thermal melting measurement through fluorescence quenching

We measured T_m of NA duplexes using the fluorescence quenching test (FQT), similar to a previous study[28]. We designed two

complementary paired single-strand NA. One strand was labeled with the FAM group at the 5′ end and its complementary strand was labeled with the BHQ1 group at the 3′ end. When the two single-stranded oligos were annealed into double-stranded NA, BHQ1 quenched the FAM fluorescence. When the NA duplexes melted during heating up, the fluorescence intensity increased due to the release of the BHQ1 strand. The peak of the derivative of the fluorescence intensity gave the T_m. The two DNA strands were FAM-GACGATCGTTCGTGAAGTCAAC and BHQ1-GTTGACTTCACGAACGATCGTG. The RNA strands have the same sequence as DNA except T bases are replaced by rU bases.

All-atom MD simulations

We performed all-atom MD simulations to probe the ion atmosphere of monovalent salts (NaCl, KCl, and CsCl) at gradient bulk concentrations (0.05 to 4 M) around DNA and RNA duplexes. We conducted the simulations using the GROMACS 2021 simulation package[56], where the OL15 force field was used to describe DNA[57] and the OL3 force field was used to represent RNA[58]. The monovalent ions were described by the parameters from the Joung and Cheatham model[59]. We ran the simulations for 600 ns after energy minimization and equilibration at 295 K and 1 bar. We used the last 500 ns of the simulation trajectory for data analysis.

oxDNA simulations

To explain how DNA duplex stability changes with salt concentration in the range of $c_{salt} < c^*_{salt}$, we conducted the CG Brownian dynamics simulations using the oxDNA simulation package[33]. The oxDNA model describes DNA electrostatic interaction using the Debye screening and has successfully reproduced many DNA properties such as DNA melting temperature (T_m). In our oxDNA simulations, the sequence of DNA hairpin is TTTTCTGGTATTTTTTTACCAGTTTT. The temperature was set to $T = 295$ K. In each simulation, we specified a salt concentration and ran 1.5×10^{10} steps. At each salt concentration, we tuned the stretching force and observed the equilibrium DNA hairpin opening/closing (Supplementary Fig. 18). We determined the critical force corresponding to the equal probability between hairpin and stretched state (Supplementary Fig. 19), same as the experimental results in Fig. 1e. We also use oxRNA model[60] to observe the zipping/unzipping of RNA hairpin. In oxRNA simulations, the sequence of the RNA is similar to that of oxDNA simulation except T is replaced by U.

CG simulations

To obtain ion distributions around DNA efficiently, we also performed CG Langevin dynamics simulations using the LAMMPS 2020 simulation package[61]. The DNA molecule was modeled as a cylinder with a uniform linear charge density of $-1e$ per 0.17 nm, and ions were modeled as hard-sphere particles. We used a $12 \times 12 \times 3.4$ nm^3 simulation box. Ions were then added to mimic salt conditions employed in MT experiments.

Reporting summary

Further information on research design is available in the Nature Portfolio Reporting Summary linked to this article.

Data availability

All data needed to evaluate the conclusions in the paper are present in the paper and the Supplementary Information. Source data for figures are provided with this paper. Source data are provided with this paper.

Code availability

The source code for MD simulations can be found via GitHub [https://github.com/cityuBiophysics/Double-stranded-Nucleic-acid-charge-inversion].

References

1. Lipfert, J., Doniach, S., Das, R. & Herschlag, D. Understanding nucleic acid–ion interactions. *Annu. Rev. Biochem.* **83**, 813–841 (2014).
2. Khimji, I., Shin, J. & Liu, J. DNA duplex stabilization in crowded polyanion solutions. *Chem. Commun.* **49**, 1306–1308 (2013).
3. Owczarzy, R., Moreira, B. G., You, Y., Behlke, M. A. & Walder, J. A. Predicting stability of DNA duplexes in solutions containing magnesium and monovalent cations. *Biochemistry* **47**, 5336–5353 (2008).
4. Vlassakis, J. et al. Probing the mechanical stability of DNA in the presence of monovalent cations. *J. Am. Chem. Soc.* **130**, 5004–5005 (2008).
5. Maity, A., Singh, A. & Singh, N. Differential stability of DNA based on salt concentration. *Eur. Biophysics. J.* **46**, 33–40 (2017).
6. Bai, Y., Das, R., Millett, I. S., Herschlag, D. & Doniach, S. Probing counterion modulated repulsion and attraction between nucleic acid duplexes in solution. *Proc. Natl Acad. Sci. USA* **102**, 1035–1040 (2005).
7. Gruenwedel, D. W. & Hsu, C.-H. Salt effects on the denaturation of DNA. *Biopolymers* **7**, 557–570 (1969).
8. Bizarro, C. V., Alemany, A. & Ritort, F. Non-specific binding of Na + and Mg 2+ to RNA determined by force spectroscopy methods. *Nucleic Acids Res.* **40**, 6922–6935 (2012).
9. Tan, Z.-J. & Chen, S.-J. Salt contribution to RNA tertiary structure folding stability. *Biophys. J.* **101**, 176–187 (2011).
10. Bloomfield, V. A. DNA condensation. *Curr. Opin. Struct. Biol.* **6**, 334–341 (1996).
11. Bloomfield, V. A. DNA condensation by multivalent cations. *Biopolymers* **44**, 269–282 (1997).
12. Besteman, K., Van Eijk, K. & Lemay, S. G. Charge inversion accompanies DNA condensation by multivalent ions. *Nat. Phys.* **3**, 641–644 (2007).
13. Shklovskii, B. I. Wigner crystal model of counterion induced bundle formation of rodlike polyelectrolytes. *Phys. Rev. Lett.* **82**, 3268–3271 (1999).
14. Grosberg, A. Y., Nguyen, T. T. & Shklovskii, B. I. Colloquium: the physics of charge inversion in chemical and biological systems. *Rev. Mod. Phys.* **74**, 329–345 (2002).
15. Hsiao, P.-Y. Overcharging, charge inversion, and reentrant condensation: using highly charged polyelectrolytes in tetravalent salt solutions as an example of study. *J. Phys. Chem. B* **112**, 7347–7350 (2008).
16. Dai, L., Mu, Y., Nordenskiöld, L. & van der Maarel, J. R. C. Molecular dynamics simulation of multivalent-ion mediated attraction between DNA molecules. *Phys. Rev. Lett.* **100**, 118301 (2008).
17. Luan, B. & Aksimentiev, A. DNA attraction in monovalent and divalent electrolytes. *J. Am. Chem. Soc.* **130**, 15754–15755 (2008).
18. Sarkar, S., Maity, A., Sarma Phukon, A., Ghosh, S. & Chakrabarti, R. Salt induced structural collapse, swelling, and signature of aggregation of two ssDNA strands: insights from molecular dynamics simulation. *J. Phys. Chem. B* **123**, 47–56 (2019).
19. Deserno, M., Jiménez-Ángeles, F., Holm, C. & Lozada-Cassou, M. Overcharging of DNA in the Presence of Salt: theory and Simulation. *J. Phys. Chem. B* **105**, 10983–10991 (2001).
20. Tomac, S. et al. Ionic effects on the stability and conformation of peptide nucleic acid complexes. *J. Am. Chem. Soc.* **118**, 5544–5552 (1996).
21. Woodside, M. T. et al. Nanomechanical measurements of the sequence-dependent folding landscapes of single nucleic acid hairpins. *Proc. Natl Acad. Sci. USA* **103**, 6190–6195 (2006).
22. Huguet, J. M. et al. Single-molecule derivation of salt dependent base-pair free energies in DNA. *Proc. Natl Acad. Sci. USA* **107**, 15431–15436 (2010).

23. Stephenson, W. et al. Combining temperature and force to study folding of an RNA hairpin. *Phys. Chem. Chem. Phys.* **16**, 906–917 (2014).
24. Bercy, M. & Bockelmann, U. Hairpins under tension: RNA versus DNA. *Nucleic Acids Res.* **43**, 9928–9936 (2015).
25. Tian, F.-J. et al. Universality in RNA and DNA deformations induced by salt, temperature change, stretching force, and protein binding. *Proc. Natl Acad. Sci. USA* **120**, e2218425120 (2023).
26. Dong, H.-L. et al. The origin of different bending stiffness between double-stranded RNA and DNA revealed by magnetic tweezers and simulations. *Nucleic Acids Res.* **120**, 2519–2529 (2024).
27. Gebala, M. & Herschlag, D. Quantitative studies of an RNA duplex electrostatics by ion counting. *Biophys. J.* **117**, 1116–1124 (2019).
28. You, Y., Tataurov, A. V. & Owczarzy, R. Measuring thermodynamic details of DNA hybridization using fluorescence. *Biopolymers* **95**, 472–486 (2011).
29. Saleh, O. A., McIntosh, D. B., Pincus, P. & Ribeck, N. Nonlinear low-force elasticity of single-stranded DNA molecules. *Phys. Rev. Lett.* **102**, 068301 (2009).
30. Chen, H. et al. Ionic strength-dependent persistence lengths of single-stranded RNA and DNA. *Proc. Natl Acad. Sci. USA* **109**, 799–804 (2012).
31. Sim, A. Y. L., Lipfert, J., Herschlag, D. & Doniach, S. Salt dependence of the radius of gyration and flexibility of single-stranded DNA in solution probed by small-angle x-ray scattering. *Phys. Rev. E* **86**, 021901 (2012).
32. SantaLucia, J. A unified view of polymer, dumbbell, and oligonucleotide DNA nearest-neighbor thermodynamics. *Proc. Natl Acad. Sci. USA* **95**, 1460–1465 (1998).
33. Šulc, P. et al. Sequence-dependent thermodynamics of a coarse-grained DNA model. *J. Chem. Phys.* **137**, 135101 (2012).
34. Cuervo, A. et al. Direct measurement of the dielectric polarization properties of DNA. *Proc. Natl Acad. Sci. USA* **111**, E3624–E3630 (2014).
35. Nguyen, T. T., Rouzina, I. & Shklovskii, B. I. Reentrant condensation of DNA induced by multivalent counterions. *J. Chem. Phys.* **112**, 2562–2568 (2000).
36. Gupta, A., Govind Rajan, A., Carter, E. A. & Stone, H. A. Ionic layering and overcharging in electrical double layers in a Poisson-Boltzmann model. *Phys. Rev. Lett.* **125**, 188004 (2020).
37. Pelta, J., Livolant, F. & Sikorav, J.-L. DNA aggregation induced by polyamines and cobalthexamine (∗). *J. Biol. Chem.* **271**, 5656–5662 (1996).
38. Yang, Y. J. et al. Cytosine methylation enhances DNA condensation revealed by equilibrium measurements using magnetic tweezers. *J. Am. Chem. Soc.* **142**, 9203–9209 (2020).
39. Dai, L., Renner, C. B. & Doyle, P. S. The polymer physics of single DNA confined in nanochannels. *Adv. Colloid Interface Sci.* **232**, 80–100 (2016).
40. Tang, J. et al. Revisiting the conformation and dynamics of DNA in slitlike confinement. *Macromolecules* **43**, 7368–7377 (2010).
41. Gupta, D. et al. Experimental evidence of weak excluded volume effects for nanochannel confined DNA. *ACS Macro Lett.* **4**, 759–763 (2015).
42. Thind, A. K. et al. Rapid cloning of genes in hexaploid wheat using cultivar-specific long-range chromosome assembly. *Nat. Biotechnol.* **35**, 793–796 (2017).
43. Moss, E. L., Maghini, D. G. & Bhatt, A. S. Complete, closed bacterial genomes from microbiomes using nanopore sequencing. *Nat. Biotechnol.* **38**, 701–707 (2020).
44. Rittich, B. & Španová, A. SPE and purification of DNA using magnetic particles. *J. Sep. Sci.* **36**, 2472–2485 (2013).
45. Aldaye, F. A., Palmer, A. L. & Sleiman, H. F. Assembling materials with DNA as the guide. *Science* **321**, 1795–1799 (2008).
46. Yang, D. et al. DNA materials: bridging nanotechnology and biotechnology. *Acc. Chem. Res.* **47**, 1902–1911 (2014).
47. Jones, M. R., Seeman, N. C. & Mirkin, C. A. Programmable materials and the nature of the DNA bond. *Science* **347**, 1260901 (2015).
48. Kumar Sharma, R., Agrawal, I., Dai, L., Doyle, P. S. & Garaj, S. Complex DNA knots detected with a nanopore sensor. *Nat. Commun.* **10**, 4473 (2019).
49. Sharma, R. K., Agrawal, I., Dai, L., Doyle, P. & Garaj, S. DNA knot malleability in single-digit nanopores. *Nano Lett.* **21**, 3772–3779 (2021).
50. Smeets, R. M. M. et al. Salt dependence of ion transport and DNA translocation through solid-state nanopores. *Nano Lett.* **6**, 89–95 (2006).
51. Howorka, S., Cheley, S. & Bayley, H. Sequence-specific detection of individual DNA strands using engineered nanopores. *Nat. Biotechnol.* **19**, 636–639 (2001).
52. Derrington, I. M. et al. Nanopore DNA sequencing with MspA. *Proc. Natl Acad. Sci. USA* **107**, 16060–16065 (2010).
53. Oren, A. Microbial life at high salt concentrations: phylogenetic and metabolic diversity. *Saline Syst.* **4**, 2 (2008).
54. Yang, Y. J. et al. A universal assay for making DNA, RNA, and RNA-DNA hybrid configurations for single-molecule manipulation in two or three steps without ligation. *ACS Synth. Biol.* **8**, 1663–1672 (2019).
55. van Loenhout, M. T. J., Kerssemakers, J. W. J., De Vlaminck, I. & Dekker, C. Non-bias-limited tracking of spherical particles, enabling nanometer resolution at low magnification. *Biophys. J.* **102**, 2362–2371 (2012).
56. Abraham, M. J. et al. GROMACS: High performance molecular simulations through multi-level parallelism from laptops to supercomputers. *SoftwareX* **1–2**, 19–25 (2015).
57. Zgarbová, M. et al. Refinement of the sugar–phosphate backbone torsion beta for AMBER force fields improves the description of Z- and B-DNA. *J. Chem. Theory Comput.* **11**, 5723–5736 (2015).
58. Zgarbová, M. et al. Refinement of the Cornell et al. nucleic acids force field based on reference quantum chemical calculations of glycosidic torsion profiles. *J. Chem. Theory Comput.* **7**, 2886–2902 (2011).
59. Joung, I. S. & Cheatham, T. E. III. Determination of alkali and halide monovalent ion parameters for use in explicitly solvated biomolecular simulations. *J. Phys. Chem. B* **112**, 9020–9041 (2008).
60. Matek, C., Šulc, P., Randisi, F., Doye, J. P. K. & Louis, A. A. Coarse-grained modelling of supercoiled RNA. *J. Chem. Phys.* **143**, 243122 (2015).
61. Thompson, A. P. et al. LAMMPS - a flexible simulation tool for particle-based materials modeling at the atomic, meso, and continuum scales. *Comput. Phys. Commun.* **271**, 108171 (2022).

Acknowledgements

We are grateful to financial support from the National Natural Science Foundation of China (No. 12074294 and 12374216 to X.-H.Z.; No. 12304254 to C.Z; No. 22273080 to L.D.), the Research Grants Council of Hong Kong (No. 11313322, 11307224 and PDFS2425-1S09), Guangdong Basic and Applied Basic Research Fund (project no. 2022A1515010484), Super Computing Center of Wuhan University, and the National Supercomputer Center in Guangzhou.

Author contributions

X.-H.Z. and L.D. conceived the idea. C.Z., J.-H.Z., W.W., and W.-Q.W. performed the experiments. L.D., F.T., H.-W.Z., and Q.-Y.Q. performed the simulations. L.D., X.-H.Z., F.T., Y.Z., Z.-J T., and W.-Q.W. analyzed the data. All authors wrote the paper.

Competing interests

The authors declare no competing interests.

Additional information

Supplementary information The online version contains supplementary material available at https://doi.org/10.1038/s41467-024-55404-6.

Correspondence and requests for materials should be addressed to Yan Zhang, Wen-Qiang Wu, Liang Dai or Xing-Hua Zhang.

Peer review information *Nature Communications* thanks Jan Lipfert, Antonio Trovato, and the other, anonymous, reviewers for their contribution to the peer review of this work. A peer review file is available.

Reprints and permissions information is available at http://www.nature.com/reprints

Publisher's note Springer Nature remains neutral with regard to jurisdictional claims in published maps and institutional affiliations.

Open Access This article is licensed under a Creative Commons Attribution-NonCommercial-NoDerivatives 4.0 International License, which permits any non-commercial use, sharing, distribution and reproduction in any medium or format, as long as you give appropriate credit to the original author(s) and the source, provide a link to the Creative Commons licence, and indicate if you modified the licensed material. You do not have permission under this licence to share adapted material derived from this article or parts of it. The images or other third party material in this article are included in the article's Creative Commons licence, unless indicated otherwise in a credit line to the material. If material is not included in the article's Creative Commons licence and your intended use is not permitted by statutory regulation or exceeds the permitted use, you will need to obtain permission directly from the copyright holder. To view a copy of this licence, visit http://creativecommons.org/licenses/by-nc-nd/4.0/.

© The Author(s) 2024